mathematics

MDPI

Article

Study of the Effect of Throttling on the Success of Starting a Line-Start Permanent Magnet Motor Driving a Centrifugal Fan

Aleksey Paramonov, Safarbek Oshurbekov, Vadim Kazakbaev, Vladimir Prakht and Vladimir Dmitrievskii *

Department of Electrical Engineering, Ural Federal University, 620002 Yekaterinburg, Russia
* Correspondence: vladimir.dmitrievsky@urfu.ru; Tel.: +7-909-028-49-25

Abstract: Direct-on-line synchronous motors are a good alternative to induction motors in fluid machinery drives due to their greater energy efficiency but have the significant disadvantage of limiting the maximum moment of inertia of the loading mechanism to ensure their successful and reliable start-up. This disadvantage is critical in centrifugal fans with a massive steel impeller. In this article, using a mathematical model, the dynamics of starting and synchronizing a permanent magnet synchronous motor fed directly from the mains as part of a fan drive are studied. The simulation results show the possibility of increasing the maximum moment of inertia of the load at the successful start-up of a direct-on-line synchronous motor by adjusting the hydraulic part of the fan pipeline by means of throttling. The conclusions of this paper can be used when selecting an electric motor to drive industrial fans and can contribute to wider use of energy-efficient synchronous motors with direct start-up from the mains.

Keywords: centrifugal fans; electric motors; energy efficiency class; energy saving; line-start permanent magnet synchronous motor; motor starting

MSC: 00A06

Citation: Paramonov, A.; Oshurbekov, S.; Kazakbaev, V.; Prakht, V.; Dmitrievskii, V. Study of the Effect of Throttling on the Success of Starting a Line-Start Permanent Magnet Motor Driving a Centrifugal Fan. *Mathematics* **2022**, *10*, 4324. https://doi.org/10.3390/math10224324

Academic Editors: Udochukwu B. Akuru, Ogbonnaya I. Okoro and Yacine Amara

Received: 7 October 2022
Accepted: 16 November 2022
Published: 18 November 2022

1. Introduction

The main function of industrial fans and blowers is to supply a large flow of air or gas at low pressure to various parts of a building or process system. They are usually driven by squirrel cage induction motors (Figure 1a). Such motors have a simple and reliable design; however, due to their operating principle, they also have a relatively high power loss, which limits their energy efficiency class [1]. For low-power induction motors in the 0.55–7.5 kW range, there are difficulties in achieving the IE4 energy efficiency class according to IEC standard 60034-30-1 "Rotating Electrical Machines—Part 30-1: Efficiency classes of line operated AC motors (IE code)" [2].

An alternative to induction motors is synchronous motors with or without permanent magnets and with a direct mains supply. This article discusses line-start permanent magnet synchronous motors (LSPMSMs, Figure 1b) [3,4]. Such motors cannot replace induction motors in the entire range of applications but have already firmly occupied some niches such as fan and pump drives [5–8]. LSPMSMs can meet the requirements of the IE4 class while retaining the dimensions of IE3 efficiency class induction motors [9].

In recent decades, the requirements for the eco-design of industrial equipment of European regulations have been tightening, namely, the requirements for the energy efficiency of electric motors [10] and the reduction of CO_2 emissions [11] are growing. The use of energy-efficient motors in industrial applications is a necessary step to achieve these goals. The goal of tightening the requirements is to achieve a climate-neutral economy [12]. Many countries have already introduced requirements for a mandatory minimum IE3 motor class: The European Union (0.75–375 kW, from 2009); Switzerland and Turkey (0.75–375 kW, from 2017); US (0.75–200 kW, since 2017); Canada (0.75–150 kW, since 2017); Mexico (0.75–375

kW, since 2010); South Korea (0.75–200 kW, since 2017); Singapore (0.75–375 kW, since 2013); Japan (0.75–375 kW, since 2014); Saudi Arabia (0.75–375 kW, since 2018); and Brazil (0.75–185 kW, since 2017) [13].

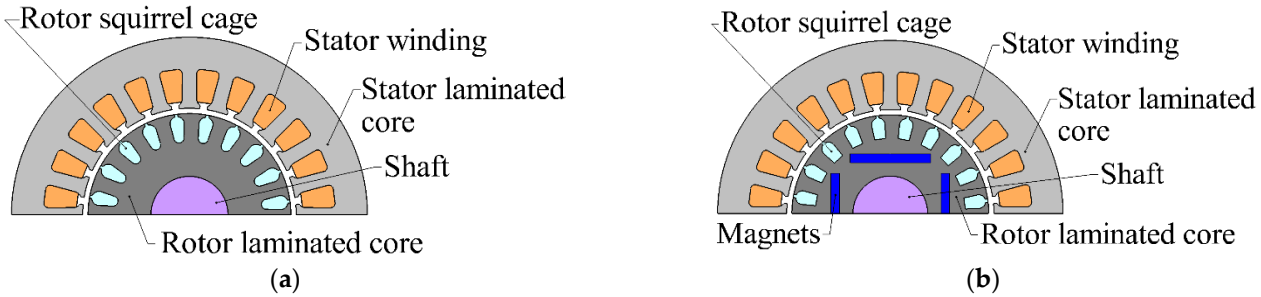

Figure 1. Motor sketches: (**a**) Induction motor (IM); (**b**) line-start permanent magnet synchronous motor (LSPMSM) [1].

LSPMSMs are commercially available from WEG [14], SEW [15], and Bharat Bijlee [16]. There are also serially produced compressors driven by LSPMSMs [17].

Induction motors usually do not have the problem of a failed start. Research on starting induction motors is usually devoted to reducing the starting time in order to reduce the motor overheating [18–20] and reducing the starting current in order to reduce the load on the network [21–23].

The identification of motor model parameters to correctly determine the starting time is often carried out by fitting the parameters using an automatic optimization method when comparing the model response with experimental starting waveforms [24]. Based on the analysis of starting waveforms and starting time, diagnostics of motor faults can also be carried out [25].

The disadvantage of LSPMSMs in comparison with induction motors is a significant limitation of the moment of inertia of the loading mechanism, which is usually indicated in the motor catalog [14,26]. This value indicates the maximum moment of inertia of the load at which the LSPMPM successfully starts and synchronizes at the rated load torque. If starting conditions are worse (exceeding load inertia and/or load torque), successful motor synchronization is not possible and, in the steady state, the motor speed is oscillatory, while the stator current exceeds the rated one by 5–7 times. Induction motors do not have such a limitation in most typical applications (fans, pumps, and compressors). The load inertia limitation requires an evaluation of the success of the synchronization during the LSPMSM start-up. There are several methods for assessing the success of the LSPMSM synchronization using: (1) Finite element model; (2) lumped-circuit model; and (3) synchronization trajectories [27,28].

The start-up simulation using the finite element model requires knowledge of the full internal structure of the LSPMSM [29], which is not always possible. The parameterization of the lumped model requires standard motor tests, such as the no-load test, short-circuit test, and load test [1,28]. The method of synchronization trajectories requires the same motor parameters for analysis as the lumped model [28]. The method of synchronization trajectories and the finite element model method have the serious drawback of being poorly suited for simulating the motor start-up in the drive of a specific mechanism. Depending on the type of driven mechanism, both the load torque and the moment of inertia reduced to the motor shaft can change during start-up. For this reason, when studying the motor start-up in the drive of a certain mechanism, it is better to use the lumped parameter model.

In most of the literature, experimental studies of LSPMSMs are carried out using laboratory benches with a load electric machine [30,31]. However, this approach does not consider the dynamic processes occurring in real applications, such as features of the mechanical characteristic of the loading mechanism (for example, the braking torque of fans and pumps is quadratically dependent on their rotation speed) and the non-linearity

of the inertia of the mechanism and fluid. Due to the lack of information on the dynamic processes in real mechanisms, when designing a drive, the motor is often oversized, which leads to a decrease in its efficiency and an increase in its cost. There are not as many articles devoted to the simulation of the operation of an LSPMSM as part of a specific mechanism, for example, a piston pump [29]. Moreover, a literature overview shows that there are no studies covering the LSPMPM start-up as part of a fan drive.

This article discusses the mathematical model of the LSPMSM as part of a centrifugal fan with a belt drive and control of the inlet vanes, as well as transients, when starting the LSPMSM powered by the mains applying fan throttling. It is known that the use of throttling in the process of starting the motor can reduce its mechanical load [27]. This article shows that this effect may be of key importance for LSPMSMs, since the impellers of the fans have a high moment of inertia, and the success of motor synchronization depends on both the moment of inertia and the braking torque of the loading mechanism. By reducing the braking torque of the fan by adjusting the inlet vanes, it is possible to ensure the start-up of the LSPMSM with a higher moment of inertia.

2. Problem Statement

Figure 2 shows the block diagram of the simulated system.

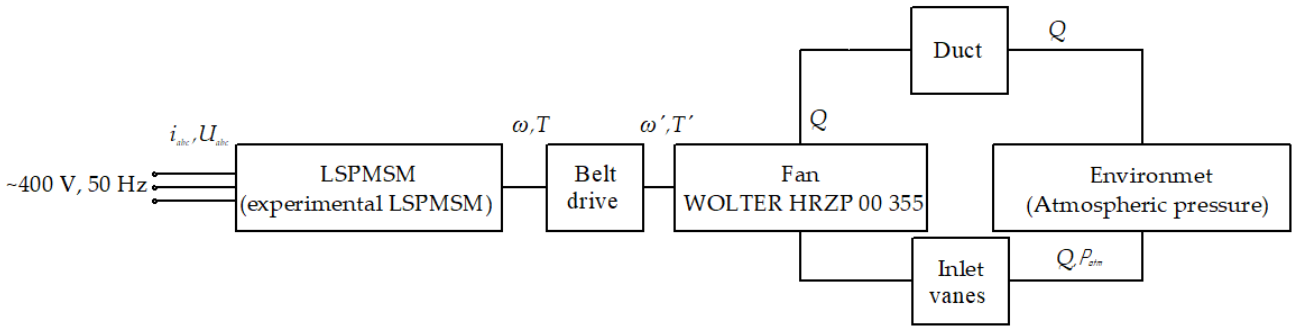

Figure 2. The block diagram of the centrifugal fan with the LSPMSM drive.

The system consists of an LSPMSM powered directly by a three-phase AC network with 400 V at 50 Hz and a serially produced centrifugal fan WOLTER HRZP 00 355 [32], the shaft of which is connected to the motor shaft through a belt drive, an inlet valve, and an air duct, through which air enters the fan from the environment and returns. This scheme is typical for separately operating fluid machines that move gas along a horizontal plane.

When modeling the system, the following assumptions were made:

- Only one fan is operating in the hydraulic system.
- All hydraulic resistances including inlet vanes (such as rooms, air ducts, air duct connections, filters, etc.) are reduced to one hydraulic diameter and reduced to one lumped element.
- There are no leaks.
- The gas is ideal and its properties are the same at every point of the duct.
- Belt drive losses are not considered.

The belt drive makes it possible to change the fan's rotational speed according to the speed of the motor [27,31]. This allows us to move the motor load closer to the rate one since the hydraulic power of the fan is proportional to the rotation speed of the third power. However, the negative side of the use of a belt drive is an additional loss [27]. Changing the fan speed causes a change in its flow–pressure curve and its dependence on the braking power on the flow, according to the laws of similarity [33]:

$$Q_2 = Q_1(n_2/n_1); \quad (1)$$

$$P_2 = P_1(n_2/n_1)^2; \quad (2)$$

$$N_{shaft\ 1} = N_{shaft\ 2}(n_2/n_1)^3, \quad (3)$$

where Q is the flow of the air; P is the static pressure rise produced by the fan; N_{shaft} is the mechanical (braking) power on the fan shaft; n is the rotational speed; index 1 denotes values without the belt drive at the fan speed indicated in the catalogue; and index 2 denotes the values after the application of the belt drive.

Throttling with inlet vanes allows for the adjustment of the operating point on the flow–pressure characteristic during the fan operation. Furthermore, this method can make it easier to start the LSPMSM, as will be shown below. The negative side is that, similar to a belt drive, throttling with inlet vanes creates an additional loss [27].

3. Mathematical Models of System Elements

3.1. LSPMSM's Mathemetical Model

For the LSPMSM mathematical model, the following assumptions are made:

- Magnetic fluxes generated by the stator and rotor windings have a sinusoidal distribution along the air gap.
- The magnetic permeability of steel is constant.
- Stator and rotor windings are symmetrical.
- Each winding is powered by a separate source.
- The supply voltage value does not depend on the load of the electrical machine.
- Losses in the magnetic core are not considered.

At each pole pitch, the LSPMSM rotor houses a permanent magnet. The axis coinciding with the direction of the magnetic flux of the magnet is denoted by q (quadrature axis). The axis perpendicular to this flux is denoted by d (direct axis). The magnet has a low value of magnetic permeability (close to 1). Therefore, the magnetic conductivity of the q-axis is less compared to the magnetic conductivity of the d-axis (Figure 3).

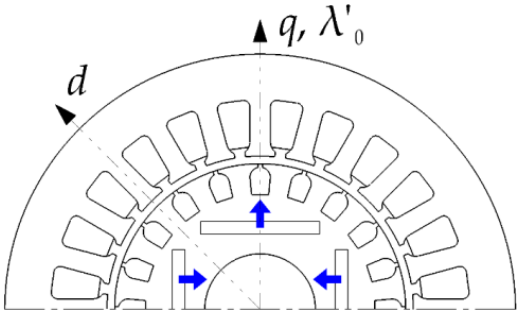

Figure 3. Directions of the d- and q-axes relative to the direction of magnetization of the permanent magnets in the rotor (shown by blue arrows).

The equations of the electrical circuits of the rotor and stator in the coordinate system associated with the rotor have the following form [34,35]:

$$\begin{aligned} d\lambda_{sd}/dt - \lambda_{sq} \cdot \omega_r + R_s \cdot I_{sd} &= U_{sd}; \\ d\lambda_{sq}/dt + \lambda_{sd} \cdot \omega_r + R_s \cdot I_{sq} &= U_{sq}; \\ d\lambda'_{rd}/dt + r'_d \cdot I'_{rd} &= 0; \\ d\lambda'_{rq}/dt + r'_q \cdot I'_{rq} &= 0, \end{aligned} \quad (4)$$

where U_{sd} and U_{sq} are the stator voltages along d- and q-axes; I_{sd}, I_{sq}, I'_{rd}, and I'_{rq} are the stator and rotor currents; λ_{sd}, λ_{sq}, λ'_{rd}, and λ'_{rq} are the stator and rotor flux linkages; ω_r is the rotor electrical angular frequency; and R_s is the stator resistance.

The rotor resistance is anisotropic, and its values along the rotor axes are designated as r'_{rd} and r'_{rq}. All rotor variables refer to the stator and therefore have a stroke in the designation. The electrical equations are supplemented by mechanical ones:

$$\begin{array}{c} J \cdot \mathrm{d}\omega_\mathrm{m}/dt = T - T_{load}; \\ \mathrm{d}\varphi/dt = \omega_\mathrm{m}, \end{array} \tag{5}$$

where $T = 3/2 \cdot Z_p \cdot (\lambda_{\mathrm{sd}} \cdot I_{sq} - \lambda_{\mathrm{sq}} \cdot I_{sd})$ represents the motor torque; T_{load} is the load torque; J is the total moment of inertia; $\omega_\mathrm{m} = \omega_\mathrm{r}/Z_p$ represents the mechanical angular frequency; φ is the mechanical rotational angle; and Z_p is the number of motor pole pairs.

The magnetic circuit equations describe the self-induction, as well as the mutual induction of the rotor and stator. Note that, due to the presence of permanent magnets, the flux linkages of the stator and rotor along the q-axis are non-zero even at zero currents [34]:

$$\begin{array}{c} \lambda'_{\mathrm{sd}} = L_{sd} \cdot I_{sd} + M_d \cdot I'_{rd}; \\ \lambda'_{\mathrm{rd}} = M_d \cdot I_{sd} + L_{rd} \cdot I'_{rd}; \\ \lambda_{\mathrm{sq}} = L_{sq} \cdot I_{sq} + M_q \cdot I'_{rq} + \lambda'_0; \\ \lambda_{\mathrm{rq}} = M_q \cdot I_{sq} + L_{rq} \cdot I'_{rq} + \lambda'_0, \end{array} \tag{6}$$

where L_{sd}, L_{sq}, L_{rd}, and L_{rq} are the stator and rotor total inductances; M_d and M_q are the stator and rotor mutual inductances; and λ'_0 is the permanent magnet flux linkage referred to as the stator.

Term λ'_0 turns out to be a free term in the expression for λ_{rq}. The free term in the expression for λ'_{rq} does not play any role, since (4) contains only the derivative of λ'_{rq}. For convenience, we will assume that the free term in the expression for λ'_{rq} is also λ'_0.

The motor is described by the system of Equations (4) and (5) with respect to ω_r, φ, λ_{sd}, λ_{sq}, λ'_{rd}, and λ'_{rq}, while the currents in (4) are considered dependencies on λ_{sd}, λ_{sq}, λ'_{rd}, and λ'_{rq}, which can be expressed in (6). Note that the currents and flux linkages of the rotor are not available for either direct or indirect measurement by simple means, such as current and voltage sensors. Rotor resistances r'_d and r'_q are not available for direct measurement with an ohmmeter. Upon substituting $\lambda_{\mathrm{rd}} = \lambda'_{\mathrm{rd}}/k$ and $I_{rd} = k \cdot I'_{rd}$, we obtain $r'_d = k^2 \cdot r_d$, $L'_{rd} = k^2 L'_{rd}$, $M'_d = k \cdot M_d$. Similarly, upon making the substitution $\lambda_{\mathrm{rq}} = \lambda'_{\mathrm{rq}}/k$ and $I_{rq} = k \cdot I'_{rq}$, we obtain $r'_q = k^2 \cdot r_q$, $L'_{rq} = k^2 \cdot L'_{rq}$, $M'_d = k \cdot M_q$, where k is a constant.

Thus, the set of parameters of the motor model is redundant, and changing the parameters by scaling the rotor currents and fluxes does not lead to a change in the dynamics of the observed values. To eliminate redundancy, we take $M_d = L_{sd}$, $M_q = L_{sq}$. Therefore, we also introduce the rotor leakage inductances $L_{\sigma d} = L_{rd} - L_{sd}$, $L_{\sigma q} = L_{rq} - L_{sq}$ only. Then (6) takes the form:

$$\begin{array}{c} \lambda_{\mathrm{sd}} = L_{sd} \cdot I_{sd} + L_{sd} \cdot I'_{rd}; \\ \lambda'_{\mathrm{rd}} = L_{sd} \cdot I_{sd} + (L_{sd} + L_{\sigma d}) \cdot I'_{rd}; \\ \lambda_{\mathrm{sq}} = L_{sq} \cdot I_{sq} + L_{sq} \cdot I'_{rq} + \lambda'_0; \\ \lambda'_{\mathrm{rq}} = L_{sq} \cdot I_{sq} + (L_{sq} + L_{\sigma q}) \cdot I'_{rq} + \lambda'_0. \end{array} \tag{7}$$

In this case, the dependencies of currents on flux links are:

$$\begin{array}{c} I'_{rd} = (\lambda'_{\mathrm{rd}} - \lambda_{\mathrm{sd}})/L_{\sigma d}; \\ I'_{rq} = (\lambda'_{\mathrm{rq}} - \lambda_{\mathrm{sq}})/L_{\sigma q}; \\ I_{sd} = \lambda_{\mathrm{sd}}/L_{sd} - I'_{rd}; \\ I_{sq} = (\lambda_{\mathrm{sq}} - \lambda'_0)/L_{sq} - I'_{rq}. \end{array} \tag{8}$$

The initial conditions for the electric circuit of Equation (4) are $I'_{rd} = I'_{rq} = I_{sd} = I_{sq} = 0$, which is expressed in terms of independent variables as follows: $\lambda'_{\mathrm{rd}} = \lambda_{\mathrm{sd}} = 0$; $\lambda'_{\mathrm{rd}} = \lambda_{\mathrm{sd}} = \lambda'_0$. Thus, upon eliminating the ambiguity, we can write the system of ordinary differential

equations for the LSPMSM complemented with the algebraic expressions to be solved in the form:

$$\begin{gathered} d\lambda_{sd}/dt - Z_p \cdot \lambda_{sq} \cdot d\varphi/dt + R_s \cdot I_{sd} = U_{sd}; \\ d\lambda_{sq}/dt + Z_p \cdot \lambda_{sd} \cdot d\varphi/dt + R_s \cdot I_{sq} = U_{sq}; \\ d\lambda'_{rd}/dt + r'_d \cdot I'_{rd} = 0; \\ d\lambda'_{rq}/dt + r'_q \cdot I'_{rq} = 0; \\ I'_{rd} = (\lambda'_{rd} - \lambda_{sd})/L_{\sigma d}; \\ I'_{rq} = (\lambda'_{rq} - [\lambda_{sq} - \lambda'_0])/L_{\sigma q}; \\ I_{sd} = \lambda_{sd}/L_{sd} - I'_{rd}; \\ I_{sq} = (\lambda_{sq} - \lambda'_0)/L_{sq} - I'_{rq}; \\ T = 3/2 \cdot Z_p \cdot (\lambda_{sd} \cdot I_{sq} - \lambda_{sq} \cdot I_{sd}); \\ J \cdot d^2\varphi/dt^2 = T - T_{load}. \end{gathered} \tag{9}$$

Figure 4 shows how the solving of this system is implemented in Simulink.

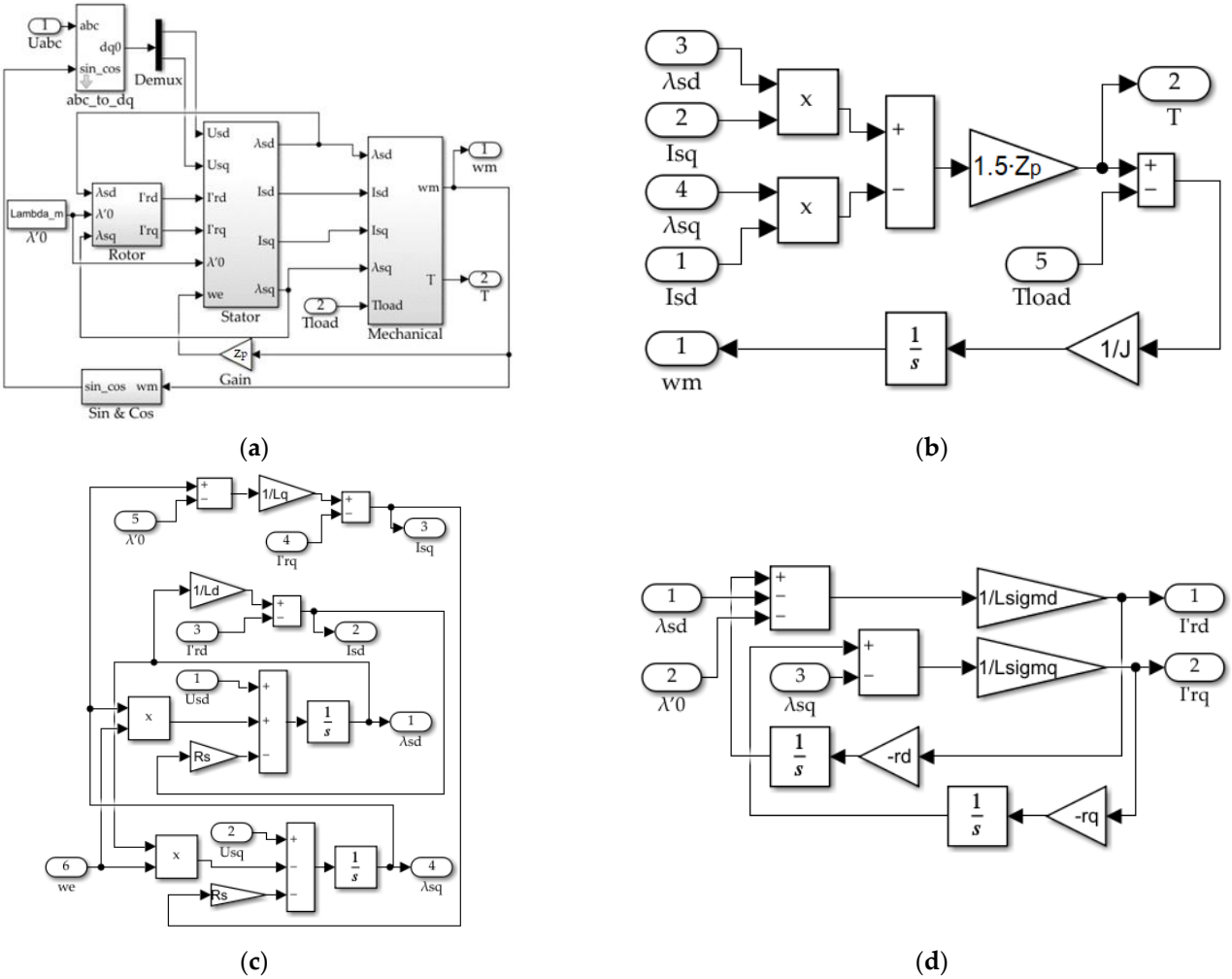

Figure 4. Simulink model of the LSPMSM motor on the *d*–*q*-axes: (**a**) General view of the model; (**b**) calculation of the motor torque and angular frequency; (**b**) calculation of stator currents; (**d**) calculation of rotor currents.

3.2. Modeling the Fan, Throttle, and Duct

The main purpose of the simulation is to determine the conditions for successful start-up and synchronization of the LSPMSM in the fan drive. Therefore, when modeling, it is important to take into account all the factors that affect the dynamics of the load at rotational speeds close to the synchronous one. At these speeds, the phase of the current with respect to the phase of the supply voltage changes slowly, and the motor mode is

replaced by a generator mode and vice versa until synchronism is achieved. Therefore, in this case, it is sufficient to use a quasi-steady model, that is, a model in which, although the hydrodynamic variables in the elements of the fluid network are assumed to be time dependent, the relationships connecting them do not depend on the previous state and do not contain time derivatives.

To simulate the hydraulic system, models from the Simscape/Fluids/Gas library of the Matlab Simulink environment were used, designed to simulate the flow of an ideal gas. The presented model uses the following gas dynamics simulation blocks: Fan (G), Pipe (G), and Fluids Local Restriction (G) [36–38].

The Fan (G) block models an adiabatic isentropic flow produced by the fan. In other words, the air can be heated due to reversible adiabatic compression by the fan. Air heating due to dissipative, irreversible processes such as viscous friction and mechanical losses of the fan are considered in the fan efficiency as decelerating torque applied to the fan shaft. The mass of air inside the fan is assumed to be negligible, and therefore inlet and outlet mass flow rates are assumed to be equal. The parameters of this block are the static pressure rise and the fan efficiency as functions of the reference parameters (the reference flow and the reference rotational speed). The static pressure rises and the fan efficiency at other flow rates and rotational speeds are calculated using the similarity laws.

The Pipe (G) block [37] is used to model the duct. This block simulates the dynamics of gas flow in a long pipeline. This considers viscous friction losses and convective heat transfer with the pipeline wall. The flow is assumed to be fully developed. Friction losses and heat transfer do not include input effects. The pipeline contains a constant volume of gas, i.e., the pipeline walls are perfectly rigid. Although the block allows for considering the change in the mass of air in the pipe due to pressure changes, the inertia of this air is not considered, which is acceptable for a quasi-stationary model of air flow.

The valve is modeled using the Fluids Local Restriction (G) block [38]. This block models the pressure drops due to a local reduction in the flow area. The processes occurring in the block are adiabatic but not isentropic (irreversible). Similar to the fan model, the air mass in this block is neglected, i.e., inlet and outlet mass flow rates are assumed to be equal. The value of the hydraulic resistance of this block can be adjusted dynamically using the "Inlet vanes" control signal. Similar to the pipeline model, this block maintains the balance of mass and energy, except for heat exchange with the environment.

Thus, although the blocks under consideration are somewhat redundant, for example, the change in the air mass in the duct due to the change in air density is insignificant, these blocks provide the necessary functionality to simulate load conditions when starting the LSPMSM as part of the fan.

4. Simulation Model of the Centrifugal Fan with the LSPMSM Drive

Figure 5 shows the block diagram of the mathematical model of the fan with the LSPMSM drive, the individual blocks of which are described in the previous section. The LSPMSM block simulating the motor is created in accordance with the system of differential Equation (9) and Figure 4. The motor is powered by a three-phase symmetrical voltage system of 400 V at 50 Hz, modeled by the Discrete 3-phase Source block.

The Fan (G) block connects the hydraulic and mechanical models. Ports A and B are connected to the hydraulic circuit (purple lines), and ports C and R are connected to the mechanical circuit (green lines). The hydraulic circuit variables are the flow and pressure. The mechanical circuit variables are the rotational speed and torque.

The load torque signal measured with the Ideal Torque Sensor at the point between the Ideal Angular Velocity Source and Fan (G) blocks is input into the LSPMSM block. The motor rotational speed calculated by the LSPMSM block is sent to the input of the Ideal Angular Velocity block through the Gain block, which simulates a belt drive and multiplies the motor speed by the gear ratio i. The Angular Velocity Source block sets the value of speed in the mechanical circuit to which the Fan (G) block is connected. The torque in this

circuit is calculated based on the given flow–pressure curve and the dependence of the fan efficiency on the flow, taking into account similarity laws (1)–(3).

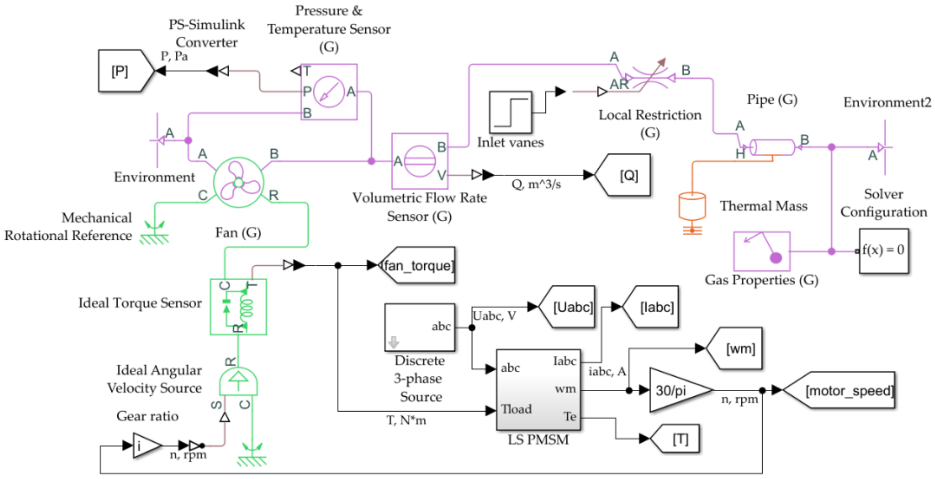

Figure 5. General view of the model of the fan with the LSPMSM drive in the Matlab Simulink.

The hydraulic part of the model consists of the fan (Fan (G) block), inlet vanes (Local Restriction block), duct (Pipe (G) block), and the environment (Environment and Environment2 blocks). The air taken from the environment under the action of the pressure rise created by the fan is regulated by the inlet vanes and, passing through the air duct, returns to the environment. Gas parameters are set in the Gas properties block. The pressure rises and flow produced by the fan are measured by the Pressure and Temperature Sensor (G) and Volumetric Flow Rate Sensor (G) blocks.

The Thermal Mass block models a thermal mass capable of accumulating internal energy [39]. The thermal mass is described by the following formula:

$$P_{thermal} = c \cdot m \cdot d\theta/dt, \tag{10}$$

where c is the specific heat capacity of a substance; m is the mass of the substance; θ is the temperature; and t is the time variable.

The blocks of this model are parameterized in such a way that the operating point of the fan in the steady state is within the flow–pressure curve reported in the manufacturer's catalog (red line in Figure 6) or within the transformed curve calculated using similarity laws (1)–(3) for a different rotational speed (for example, the blue line in Figure 6) [32].

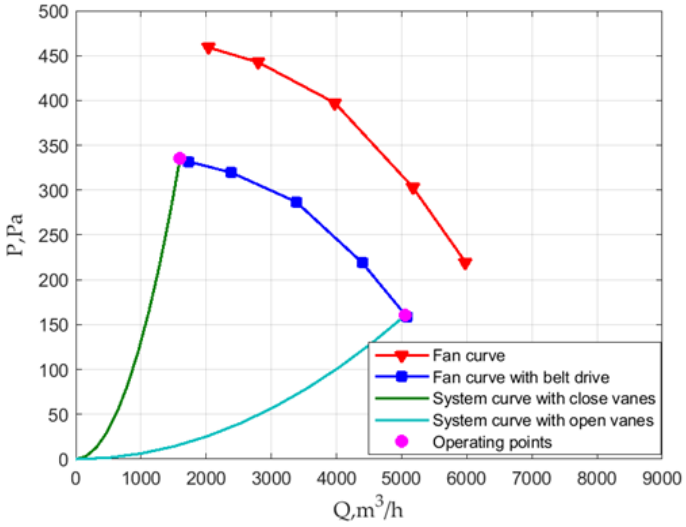

Figure 6. Flow–pressure curves of the fan with and without belt drive, as well as the duct curves with open and closed inlet vanes.

Table 1 shows the parameters of the LSPMSM with a rated power of 0.55 kW and a rated speed of 1500 rpm used for the simulation.

Table 1. LSPMSM parameters.

Parameter	Value
Rated power P_{rate}, kW	0.55
Rated line-to-line voltage U_{rate}, V	380
Rated frequency f, Hz	50
Pole pair number Z_p	2
Stator phase resistance R_s, Ohm	15.3
Total direct inductance L_{sd}, H	0.26
Total quadrature inductance L_{sq}, H	0.15
Leakage direct inductance $L_{\sigma d}$, H	0.038
Leakage quadrature inductance $L_{\sigma q}$, H	0.051
Rotor direct resistance r'_d, Ohm	9.24
Rotor quadrature resistance r'_q, Ohm	10.1
Permanent magnet flux linkage λ'_0, Wb	0.76
Motor inertia moment J_m, kg·m^2	0.003
Fan impeller inertia moment J_i, kg·m^2	0.06

To simulate the fan, the parameters of a commercially produced centrifugal fan WOLTER HRZP 00 355 with a moment of inertia J_i = 0.1 kg·m^2 and characteristics shown in Table 2 according to [32] were used. This fan involves the use of a belt drive. For this study, the gear ratio i = 0.85 of the belt drive was selected. Figure 6 shows the flow–pressure characteristics of the fan without and with the use of a belt drive, as well as the curves of the duct at various positions of the inlet vanes: $S_{valve} = S$ (fully open) and $S_{valve} = 0.25 \cdot S$ (fully closed). The cross-sectional area of the duct is equal to S_{duct} = 0.099 m^2, and the length of the duct is equal to l_{duct} = 30 m.

Table 2. Fan characteristics.

Flow Q, m^3/h	Pressure P, Pa	Fan Hydraulic Efficiency η, %
2035	459	64
2803	442	75
3977	397	79
5170	303	78
5981	219	58

5. Simulation Results

The LSPMSM start-up simulation is carried out for two different cases:

(1) When the inlet vanes are fully open (the control signal of the inlet valve is maximum $S_{valve} = S$).

(2) When dynamically changing the valve position, corresponding to the following algorithm: $S_{valve} = 0.25 \cdot S$ at t < 4 s (this value of the control signal corresponds to the minimum fan flow from the flow–pressure curve given for the considered fan type in the catalog [32], which models the fan operation with a fully closed valve; this assumption is made due to the lack of information about the fan braking torque at lower flow rates) and $S_{valve} = S$ at t $\geq$ 4. Figures 7–12 show the simulation results for both cases.

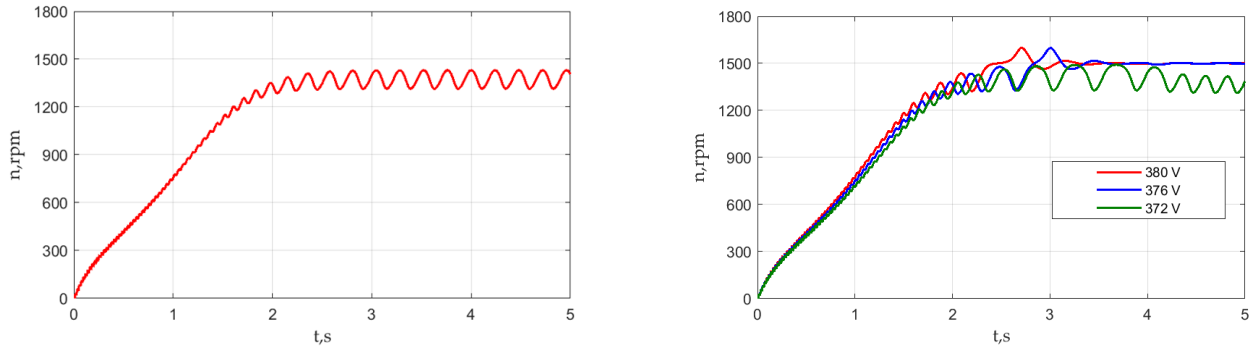

(**a**) (**b**)

Figure 7. LSMPM rotational speed versus time: (**a**) Fully open valve, 380 V; (**b**) fully closed valve, various voltages.

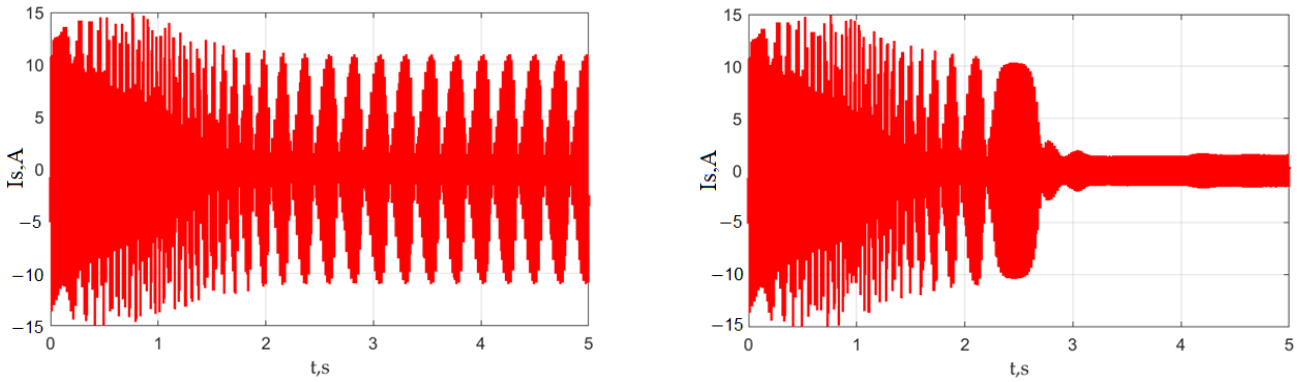

(**a**) (**b**)

Figure 8. LSPMSM stator current versus time, 380 V: (**a**) Fully open valve; (**b**) fully closed valve.

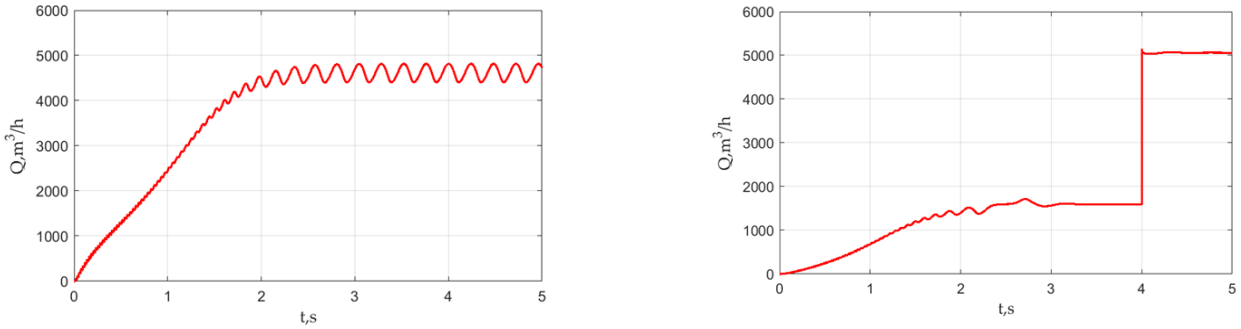

(**a**) (**b**)

Figure 9. Flow versus time, 380 V: (**a**) Fully open valve; (**b**) fully closed valve.

Figure 7a shows that with $S_{valve} = S$, the motor reaches a speed of approximately ≈ 1350 rpm in approximately 2 s but cannot accelerate to a synchronous speed of 1500 rpm. Next, quasi-steady oscillations in speed begin with a maximum value of 1430 rpm, a minimum value of 1315 rpm, and an average value of 1408 rpm. Thus, starting the motor in this case is unsuccessful.

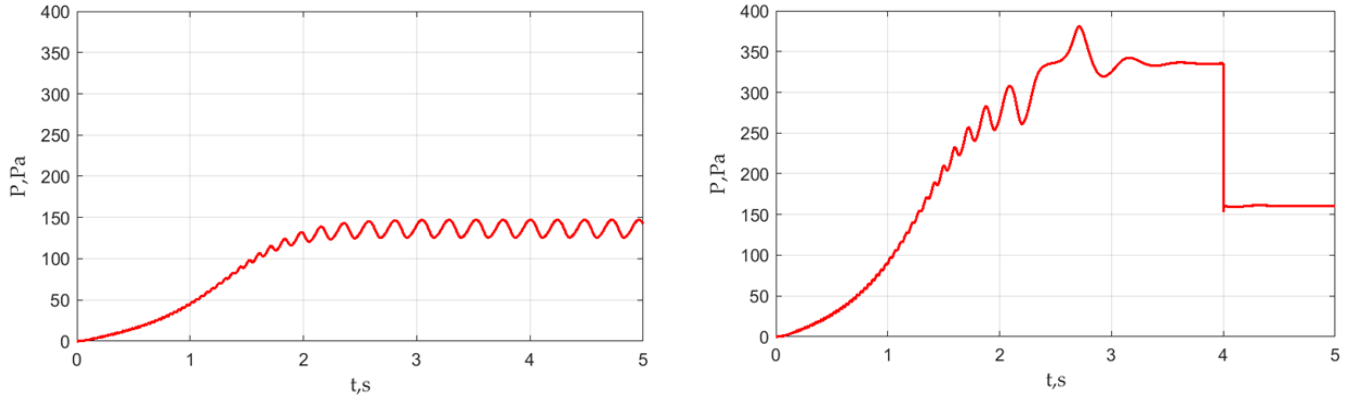

(**a**) (**b**)

Figure 10. Pressure versus time, 380 V: (**a**) Fully open valve; (**b**) fully closed valve.

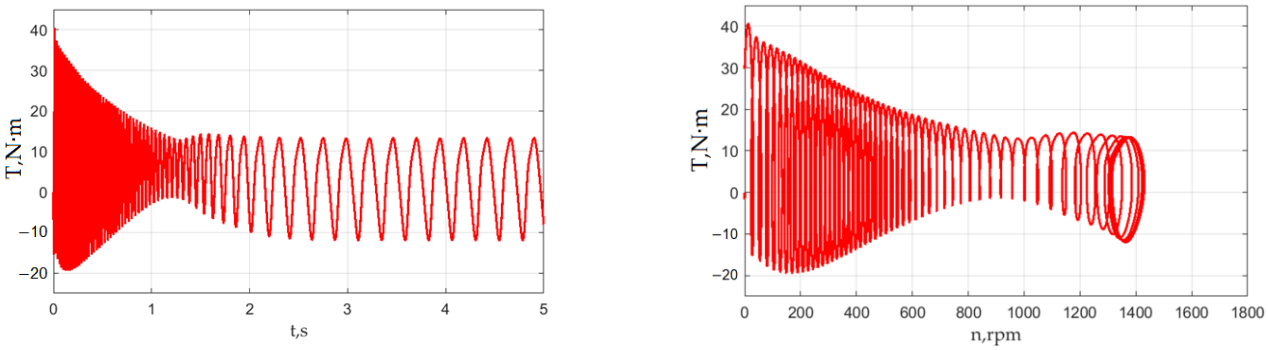

(**a**) (**b**)

Figure 11. LSPMSM torque with fully open valve, 380 V: (**a**) Torque versus time; (**b**) torque versus speed.

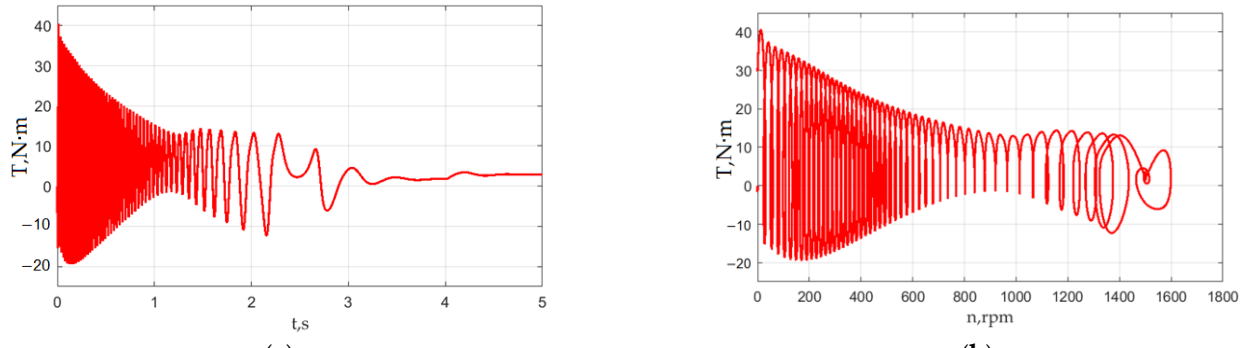

(**a**) (**b**)

Figure 12. LSPMSM torque with fully closed valve, 380 V: (**a**) Torque versus time; (**b**) torque versus speed.

The red line in Figure 7b shows the motor speed waveform at the rated voltage when starting with the valve closed ($S_{valve} = 0.25 \cdot S$). In this case, the motor successfully synchronizes, reaching a steady speed of 1500 rpm in approximately 3.5 s. After the opening of the inlet vanes (load surge) at the time t = 4 s, the speed first decreases to 1493 rpm. Then, after 0.5 s, the synchronous speed of 1500 rpm is restored.

The blue line in Figure 7b shows the speed waveform with a voltage drop of 1%. In this case, the motor still starts successfully, although the start time is slightly longer. The green line shows the speed waveform with a voltage drop of 2%. In this case, although the motor reaches 1500 rpm, it then falls out of synchronism, and the process of being pulled in and out of synchronism is periodically repeated. After a load surge at time t = 4 s, the motor starts to operate in an asynchronous mode without reaching the synchronous speed.

Figures 8–10 show the current, flow, and pressure transients at various valve positions at the rated supply voltage. Figure 8a shows a waveform of the phase current of the motor during the failed synchronization. In this case, the steady current amplitude is variable and depends on the instantaneous speed. The maximum instantaneous current of the LSPMSM in the quasi-steady state is 10.5 A, which exceeds the current amplitude during normal operation by 6.7 times (10.6/1.56 = 6.7, see below). With the prolonged operation, such a current will certainly lead to the failure of the motor. Figure 8b shows the current waveform with the valve closed during the start-up. In this case, the start and synchronization take 3.5 s. The amplitude of the steady current after the synchronization is 1.44 A. After opening the valve, the amplitude of the current increases to 1.56 A.

Figure 9a shows the waveform of the fan volumetric air flow with the inlet vanes fully open. Since the flow is proportional to the fan speed (1), this transient follows the motor speed waveform, which also takes place due to the low inertia of the gas. The flow has a quasi-steady oscillatory character with a maximum of 4809 m^3/h, a minimum of 4408 m^3/h, and an average of 4609 m^3/h. Figure 9b shows the waveform of the flow with the valve closed during start-up. The flow rate gradually increases from 0 to 1600 m^3/h as the motor accelerates to its synchronous speed. As noted above, the presence of the non-zero flow rate at a fully closed valve is an assumption of this model, made due to the lack of information about the fan braking torque at lower flow rates, which does not affect the main conclusions of the article. After opening the valve, the flow through the fan increases several times up to 5000 m^3/h. Opening the valve after the motor has reached a synchronous speed causes a step change in the flow. This step response is due to the low inertia of the gas.

Figure 10a shows the fan pressure rise waveform with the valve open. Due to the quadratic dependence of pressure on the fan speed (2), this transient follows the motor speed waveform but has a large amplitude of the oscillatory component. The maximum value in the quasi-steady operation is 146.67 Pa, the minimum is 125.67 Pa, and the average is 136.17 Pa. Figure 10b shows the waveform of the pressure with the valve closed during start-up. Opening the inlet vanes causes a stepwise decrease in the pressure. The steady pressure before opening the valve is 335 Pa, and after opening it is 160.61 Pa.

Figures 11–14 show plots of the motor torque versus time and speeds for the various cases under consideration.

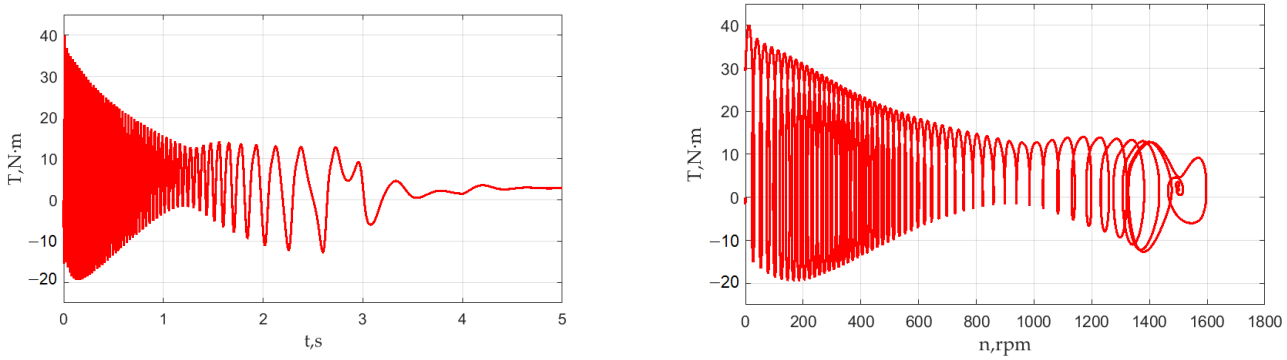

(**a**) (**b**)

Figure 13. LSPMSM torque with fully closed valve, 376 V: (**a**) Torque versus time; (**b**) torque versus speed.

Figure 11 shows the torque waveforms with a fully open valve and a 380 V supply voltage. Since the LSPMSM operates in an asynchronous mode due to unsuccessful synchronization, the torque has a large oscillatory component with a maximum of 13.1 N·m, a minimum of −11.87 N·m, and an average of 0.62 N·m. In this case, the presence of torque and speed oscillations (see the speed waveform in Figure 7a and the torque waveform in Figure 11a) is due to the fact that the LSPMSM operates in an asynchronous mode. During the initial startup phase, the LSPMSM runs in an asynchronous mode. In this mode, the positive torque, due to which the motor accelerates, is the asynchronous torque of the short-

circuited cage, and the magnets create an oscillatory alternating torque. If the moment of inertia is too large, the speed oscillations are smoothed out, and the LSPMSM operates with some slip, similarly to an asynchronous motor, i.e., does not reach the synchronous speed.

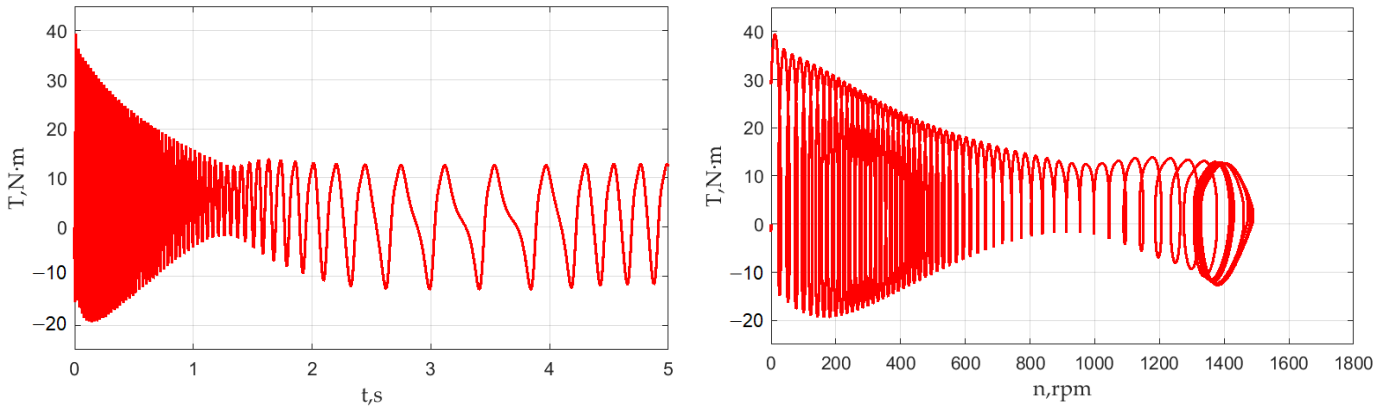

(**a**) (**b**)

Figure 14. LSPMSM torque with fully closed valve, 372 V: (**a**) Torque versus time; (**b**) torque versus speed.

If the inertia is not too large or the load torque is low, the speed oscillations caused by torque oscillations increase. If the speed oscillations are sufficient to achieve a synchronous speed (as in the case shown in Figures 7b and 12a), then the synchronization process begins. In this process, the motor first overshoots the synchronous speed (see Figure 7b, red and blue lines at $t \approx 3$ s) and then settles down, i.e., the speed stabilizes and becomes equal to the synchronous speed. The critical moment of inertia of the loading mechanism (the moment of inertia of the loading mechanism at which an LSPMSM is able to start at the rated load torque) is indicated in the catalogs of mass-produced LSPMSMs [14,15].

Figure 12 shows the torque waveform with the valve closed at start-up. After successful synchronization, the motor torque has a constant value. The steady torque before opening the valve is 3.91 N·m and is 4.9 N·m after opening the valve. Figures 13 and 14 show torque plots for starting the motor with the fully closed valve at 1% and 2% voltage drops, respectively.

6. Conclusions

In this study, a mathematical model was developed to investigate the starting performance of a line-start permanent magnet synchronous motor (LSPMSM) as part of an industrial centrifugal fan drive. This mathematical model evaluated the critical moment of inertia and the static torque of the loading mechanism, exceeding which makes successful synchronization during the start-up process impossible.

The simulation was carried out using the parameters of a 0.55 kW 1500 rpm LSPMSM and a serially produced fan. The comparison of dynamic processes and simulation results of the motor start-up in a fan drive with and without air flow control by inlet vanes was carried out. It was shown that closing the inlet valve at start-up facilitates synchronization of the LSPMSM and increases the maximum moment of inertia at which the fan starts successfully.

When the fan moment of inertia is high (exceeding the critical moment of inertia of the motor), which cannot be reduced by a belt drive, and the static load torque is close to the rated one, the LSPMSM cannot successfully synchronize. Long-term operation of LSPMSMs in asynchronous mode leads to large current overloads, overheating, and, ultimately, motor failure. Therefore, the asynchronous mode is unacceptable for the long-term operation of LSPMSMs.

However, as shown by the simulation results presented in the article, in this case, successful synchronization can be achieved by throttling the fan duct. Closing the inlet

valve at start-up contributes to the successful synchronization of the LSPMSM. After the motor start-up, the valve can be opened again.

The results of this study can be used to select a more energy-efficient fan drive motor, even if the starting characteristics of the motor specified in the manufacturer's catalog are not satisfactory for a given application. In future works, the start-up of fluid-processing mechanisms employing direct-on-line synchronous motors at reduced voltages and with long cable lengths will be investigated.

Author Contributions: Conceptual approach, A.P., V.K. and V.P.; data duration, A.P. and S.O.; software, A.P., S.O. and V.K.; calculations and modeling, A.P., S.O., V.D., V.K. and V.P.; writing—original draft, A.P., S.O., V.D., V.K. and V.P.; visualization, A.P. and V.K.; review and editing, A.P., S.O., V.D., V.K. and V.P. All authors have read and agreed to the published version of the manuscript.

Funding: The work was partially supported by the Ministry of Science and Higher Education of the Russian Federation (through the basic part of the government mandate, Project No. FEUZ 2020-0060).

Data Availability Statement: Data are contained within the article.

Acknowledgments: The authors thank the editors and reviewers for careful reading and constructive comments.

Conflicts of Interest: The authors declare no conflict of interest.

References

1. Kazakbaev, V.; Paramonov, A.; Dmitrievskii, V.; Prakht, V.; Goman, V. Indirect Efficiency Measurement Method for Line-Start Permanent Magnet Synchronous Motors. *Mathematics* **2022**, *10*, 1056. [CrossRef]
2. Rotating Electrical Machines—Part 30-2: Efficiency Classes of Variable Speed AC Motors (IE-Code). IEC 60034-30-2/ IEC: 2016-12. Available online: https://webstore.iec.ch/publication/30830 (accessed on 6 October 2022).
3. Liu, C. Rotor Conductor Arrangement Designs of High-Efficiency Direct-on-Line Synchronous Reluctance Motors for Metal Industry Applications. *IEEE Trans. Ind. Appl.* **2020**, *56*, 4337–4344. [CrossRef]
4. Ding, T.; Takorabet, N.; Sargos, F.; Wang, X. Design and Analysis of Different Line-Start PM Synchronous Motors for Oil-Pump Applications. *IEEE Trans. Magn.* **2009**, *45*, 1816–1819. [CrossRef]
5. Goman, V.; Oshurbekov, S.; Kazakbaev, V.; Prakht, V.; Dmitrievskii, V. Energy Efficiency Analysis of Fixed-Speed Pump Drives with Various Types of Motors. *Appl. Sci.* **2019**, *9*, 5295. [CrossRef]
6. Baka, S.; Sashidhar, S.; Fernandes, B.G. Design of an Energy Efficient Line-Start Two-Pole Ferrite Assisted Synchronous Reluctance Motor for Water Pumps. *IEEE Trans. Energy Conv.* **2021**, *36*, 961–970. [CrossRef]
7. Ismagilov, F.; Vavilov, V.; Gusakov, D. Line-Start Permanent Magnet Synchronous Motor for Aerospace Application. In Proceedings of the 2018 IEEE International Conference on Electrical Systems for Aircraft, Railway, Ship Propulsion and Road Vehicles and International Transportation Electrification Conference (ESARS-ITEC 2018), Nottingham, UK, 7–9 November 2018; pp. 1–5. [CrossRef]
8. Kurihara, K.; Rahman, M. High-Efficiency Line-Start Interior Permanent-Magnet Synchronous Motors. *IEEE Trans. Ind. Appl.* **2004**, *40*, 789–796. [CrossRef]
9. Kazakbaev, V.; Prakht, V.; Dmitrievskii, V.; Golovanov, D. Feasibility Study of Pump Units with Various Direct-On-Line Electric Motors Considering Cable and Transformer Losses. *Appl. Sci.* **2020**, *10*, 8120. [CrossRef]
10. European Commission Regulation (EC), No. 640/2009 Implementing Directive 2005/32/ EC of the European Parliament and of the Council with Regard to Ecodesign Requirements for Electric Motors, (2009), Amended by Commission Regulation (EU) No 4/2014 of January 6, 2014. Document 32014R0004. Available online: https://eur-lex.europa.eu/legal-content/EN/TXT/?uri=CELEX%3A32014R0004 (accessed on 6 October 2022).
11. European Council Meeting (10 and 11 December 2020)—Conclusions. EUCO 22/20 CO EUR 17 CONCL 8. Available online: https://www.consilium.europa.eu/media/47296/1011-12-20-euco-conclusions-en.pdf (accessed on 6 October 2022).
12. The European Green Deal. Available online: https://ec.europa.eu/info/strategy/priorities-2019-2024/european-green-deal_en (accessed on 6 October 2022).
13. Goman, V.; Prakht, V.; Kazakbaev, V.; Dmitrievskii, V. Comparative Study of Induction Motors of IE2, IE3 and IE4 Efficiency Classes in Pump Applications Taking into Account CO_2 Emission Intensity. *Appl. Sci.* **2020**, *10*, 8536. [CrossRef]
14. WQuattro, Super Premium Efficiency Motor, Product Catalogue, WEG Group—Motors Business Unit, Cod: 50025713, Rev: 03, Date (m/y): 07/2017. Available online: https://static.weg.net/medias/downloadcenter/h01/hfc/WEG-w22-quattro-european-market-50025713-brochure-english-web.pdf (accessed on 6 October 2022).
15. Addendum to the Operating Instructions: AC Motors DR.71.J-DR.100.J with LSPM Technology, 21281793/EN, 09/2014, SEW Eurodrive. Available online: https://download.sew-eurodrive.com/download/pdf/21343799.pdf (accessed on 6 October 2022).

16. Catalogue of Super Premium Efficiency SynchroVERT LSPM Motors. Available online: https://www.bharatbijlee.com/media/14228/synchrovert_catalogue.pdf (accessed on 6 October 2022).
17. KT-420-5, Operation of Bitzer reciprocating compressors with external frequency inverters, Bitzer, 01.2022. Available online: https://www.bitzer.de/shared_media/html/kt-420/Resources/pdf/279303819.pdf (accessed on 6 October 2022).
18. Grag, A.; Tomar, A. Starting Time Calculation for Induction Motor. *J. Electr. Electron. Syst.* **2015**, *4*, 149. [CrossRef]
19. Xia, Y.; Han, Y.; Xu, Y.; Ai, M. Analyzing Temperature Rise and Fluid Flow of High-Power-Density and High-Voltage Induction Motor in the Starting Process. *IEEE Access* **2019**, *7*, 35588–35595. [CrossRef]
20. Dems, M.; Komeza, K.; Szulakowski, J.; Kubiak, W. Dynamic Simulation of High-Speed Induction Motor. *Energies* **2021**, *14*, 2713. [CrossRef]
21. Aree, P. Starting time calculation of large induction motors using their manufacturer technical data. In Proceedings of the 2016 19th International Conference on Electrical Machines and Systems (ICEMS), Chiba, Japan, 13–16 November 2016; pp. 1–5. Available online: https://ieeexplore.ieee.org/document/7837339 (accessed on 6 October 2022).
22. Digalovski, M.; Rafajlovski, G. Calculation of Starting and Breaking Times of Induction Motor Electric Drives, for Different Mechanical Loads. In Proceedings of the 2020 International Conference on Information Technologies (InfoTech), Varna, Bulgaria, 17–18 September 2020; pp. 1–4. [CrossRef]
23. Maleki, M.G.; Chabanloo, R.M.; Farrokhifar, M. Accurate coordination method based on the dynamic model of overcurrent relay for industrial power networks taking contribution of induction motors into account. *IET Gener. Transm. Distrib.* **2020**, *14*, 645–655. [CrossRef]
24. Guedes, J.J.; Castoldi, M.F.; Goedtel, A.; Agulhari, C.M.; Sanches, D.S. Parameters estimation of three-phase induction motors using differential evolution. *Electr. Power Syst. Res.* **2018**, *154*, 204–212. [CrossRef]
25. Faiz, J.; Ebrahimi, B.M.; Akin, B.; Toliyat, H.A. Finite-Element Transient Analysis of Induction Motors Under Mixed Eccentricity Fault. *IEEE Trans. Magn.* **2008**, *44*, 66–74. [CrossRef]
26. Abdoulkadri, C.; Albert, J.; Wang, S.; Wang, R. Analytical Synchronization Analysis of Line-Start Permanent Magnet Synchronous Motors. *Prog. Electromagn. Res. M* **2016**, *48*, 183–193. [CrossRef]
27. Barkeley, L. Improving Fan System Performance. A Sourcebook for Industry. U.S. Department of Energy. 2003; DOE/GO-102003-1294. Available online: https://www.nrel.gov/docs/fy03osti/29166.pdf (accessed on 6 October 2022).
28. Soulard, J.; Nee, H. Study of the synchronization of line-start permanent magnet synchronous motors. In Proceedings of the 2000 IEEE Industry Applications Conference. Thirty-Fifth IAS Annual Meeting and World Conference on Industrial Applications of Electrical Energy (Cat. No.00CH37129), Rome, Italy, 8–12 October 2000; pp. 424–431. [CrossRef]
29. Poudel, B. Line Start Permanent Magnet Synchronous Motor for Multi Speed Application. Master Thesis, University of New Orleans, New Orleans, LA, USA, 2017. Available online: https://scholarworks.uno.edu/td/2430 (accessed on 6 October 2022).
30. Kahrisangi, M.; Hassanpour, I.; Zadeh, A.; Zadeh, V.; Mohammad, S.; Mohammad, R. Line-start permanent magnet synchronous motors versus induction motors: A comparative study. *Front. Electr. Electron. Eng.* **2012**, *7*, 459–466. [CrossRef]
31. Cory, W. *Fans & Ventilation: A Practical Guide*; Elsevier Science: Amsterdam, The Netherlands, 2005.
32. Centrifugal Fans. Wolter GmbH+Co KG. M08.6. V.2006/1. Available online: https://www.wolter.eu/fileadmin/BILDER/produkte/5-radialventilatoren/pdf/Radialventilator_TRZ_HRZ_HRZP.pdf (accessed on 6 October 2022).
33. Rory, A.R.; Scott, M. Modeling Techniques for a Computational Efficient Dynamic Turbofan Engine Model. *Int. J. Aerosp. Eng.* **2014**, *2014*, 283479. [CrossRef]
34. Wang, D.; Wang, X.; Chen, H.; Zhang, R. Matlab/Simulink-Based Simulation of Line-start PMSM Used in Pump Jacks. In Proceedings of the IEEE Conference on Industrial Electronics and Applications, Harbin, China, 23–25 May 2007; pp. 1179–1181. [CrossRef]
35. Modeer, T. Modeling and Testing of Line Start Permanent Magnet Motors. Ph.D. Thesis, School of Electrical Engineering, KTH, Stockholm, Sweden, 2007. Available online: https://citeseerx.ist.psu.edu/viewdoc/download?doi=10.1.1.826.9539&rep=rep1&type=pdf (accessed on 6 October 2022).
36. Mathworks. Fan (G), Fan in Gas Network. Model Description. Available online: https://www.mathworks.com/help/hydro/ref/fang.html;jsessionid=dd48cc776badaa81163a0d6aa2ff (accessed on 6 October 2022).
37. Mathworks. Pipe (G), Rigid Conduit for Gas Flow. Model Description. Available online: https://www.mathworks.com/help/simscape/ref/pipeg.html (accessed on 6 October 2022).
38. Mathworks. Local Restriction (G), Restriction in Flow Area in Gas Network. Model Description. Available online: https://www.mathworks.com/help/simscape/ref/localrestrictiong.html (accessed on 6 October 2022).
39. Mathworks. Thermal Mass, Mass in Thermal Systems. Model Description. Available online: https://www.mathworks.com/help/simscape/ref/thermalmass.html (accessed on 6 October 2022).